First-Principles Prediction of the Equilibrium Shape of Nanoparticles Under Realistic Electrochemical Conditions

Nicéphore Bonnet[1] and Nicola Marzari[2]

[1]Department of Materials Science and Engineering, MIT, Cambridge, Massachusetts 02139, USA

[2]Theory and Simulation of Materials, École Polytechnique Fédérale de Lausanne, Station 12, 1015 Lausanne, Switzerland

(Received 30 October 2012; published 20 February 2013)

A first-principles model of the electrochemical double layer is applied to study surface energies and surface coverage under realistic electrochemical conditions and to determine the equilibrium shape of metal nanoparticles as a function of applied potential. The potential bias is directly controlled by adding electronic charge to the system, while total energy calculations and thermodynamic relations are used to predict electrodeposition curves and changes in surface energies and coverage. This approach is applied to Pt surfaces subject to hydrogen underpotential deposition. The shape of Pt nanoparticles under a cathodic scan is shown to undergo an octahedric-to-cubic transition, which is more pronounced in alkaline media due to the interaction energy of the *p*H-dependent surface charge with the surface dipole.

DOI: 10.1103/PhysRevLett.110.086104 PACS numbers: 82.45.Fk, 82.45.Jn, 82.47.−a, 82.60.Qr

Electrocatalysis plays a fundamental role in the harvesting, storage, and transformation of energy, as well as in many processes of great technological importance—from gas generation to corrosion to metal processing [1]. In particular, electrochemical conversion of fuels into electricity depends critically on nanostructured catalysts that are often based on rare or precious metals [2], and ongoing research aims at designing new materials for fuel cell electrodes exhibiting an improved tradeoff between efficiency, chemical stability, and cost [3]. Theoretical calculations have been very successful in addressing reaction mechanisms and activation barriers under ultrahigh vacuum conditions [4,5] and have been increasingly emphasizing the importance of bridging the gap between ideal and realistic operating conditions, where the effects of temperature, partial pressure, and applied potential on the stability and activity of catalysts are accounted for [6–9]. The study of perfect single crystals has highlighted the role of facet orientation in determining reactivity [10], and simulations have been successively applied to extract valuable predictors [11,12], while others have related improved catalytic activities to a reduction in adsorbate surface coverage mitigating the site-blocking effect [13]. More recently, theoretical calculations have focused on understanding the role of the applied electrochemical potential, the presence of a solvent and electrolytes, and the nature of the double layer in determining catalytic activity [14–21].

In this Letter, a first-principles model of the double layer is used to simulate surfaces in realistic electrochemical conditions [20,21], and total energy calculations and thermodynamic relations are combined to predict electrodeposition curves and surface energies as a function of coverage, leading to the determination of the equilibrium shapes of nanoparticles as a function of applied potential and *p*H. This approach is applied to Pt nanoparticles during hydrogen underpotential deposition, showing good agreement with available experimental data. More broadly, this work highlights the interdependence of key factors in electrocatalysis—namely, electric bias, adsorbate coverage, and catalyst geometry.

Following the approach of Ref. [22], the electrosorption of the proton ($H^+ + e^- \rightarrow H^*$) is decomposed into the two-step process

$$H^+_{aq} + e^- \rightarrow \frac{1}{2} H_2(g) \tag{1}$$

and

$$\frac{1}{2} H_2(g) \rightarrow H^*. \tag{2}$$

By definition, the first reaction is at equilibrium when the working electrode is at the potential of the reversible hydrogen electrode (Φ_{RHE}). Therefore, at a potential U measured with respect to the RHE, the overall free energy change upon electrosorption of one proton is

$$\Delta G_{tot} = eU + \Delta G(\theta) + kT \ln \frac{\theta}{1-\theta}, \tag{3}$$

where $\Delta G(\theta)$ is the free energy of reaction (2) as a function of hydrogen coverage θ and the last term accounts for the change in the configurational entropy of the surface. In turn, $\Delta G(\theta)$ is computed as

$$\Delta G(\theta) = \Delta E + \Delta E_{zpe} + TS,$$

with $-TS$ being the entropic free energy of $\frac{1}{2} H_2$ in the gas phase (-0.20 eV at room temperature and atmospheric pressure [23]), whereas ΔE and ΔE_{zpe} are the changes, upon adsorption, in the total energy and the vibrational zero-point energy, respectively.

Total energies and vibrational properties are calculated using density functional theory (DFT), as implemented in the QUANTUM-ESPRESSO distribution [24]. The metal surface is represented by a four-layer slab in the (111) or (100)

direction with an equilibrium lattice parameter of 4.0 Å. Adsorption energies are computed for a $(2 \times \sqrt{3})$ unit cell, with H being placed at the preferential site, i.e., the fcc site on (111) and the bridge site on (100), and relaxing the topmost metal layer. The Perdew-Burke-Ernzerhof exchange-correlation functional [25] is used, in combination with ultrasoft pseudopotentials for the ion cores [26]. We use a plane-wave cutoff of 30 Ry and a $7 \times 7 \times 1$ k-point mesh with 0.01 Ry of cold smearing [27] for converged Brillouin zone sampling.

The electrode potential is controlled by adding explicit charges on the slab [14,20], and a corrective potential is applied, as discussed in Ref. [28], to remove undesired periodic-image interactions. The electrochemical double layer is modeled by placing a planar countercharge at a distance of 3 Å from the metal surface. The dipolar response of water is rendered by inserting a continuum dielectric medium inside the double layer [29]. Cyclic voltammetry and impedance spectroscopy measurements in 0.1–1 M electrolytes have yielded a double-layer capacitance c_{dl} in the range 20–100 $\mu\mathrm{F/cm^2}$ [30]. Here, a representative value of 40 $\mu\mathrm{F/cm^2}$ is chosen, which, for the geometry considered, implies a relative permittivity of 13.6, consistent with a previous estimate from molecular dynamics simulations [31]. Finally, the absolute electrode potential Φ is computed as $-v(\infty) - \epsilon_F/e$, where $v(\infty)$ is the value of the electrostatic potential in the flat region outside the double layer and ϵ_F is the Fermi energy. Since this model ignores the chemical effects of water, and in particular its contribution to the surface dipole, the potential of zero charge (PZC) is taken from experimental measures. The CO charge displacement method gives $\Phi_{\mathrm{PZC}} \simeq 0.23$ V/SHE [32], where the standard hydrogen electrode (SHE) is by definition a reversible hydrogen electrode in which the pH is set to 0. Other measurements by impedance spectroscopy suggest $\Phi_{\mathrm{PZC}} \simeq 0.34$ V/SHE [30]. Incidentally, those values happen to be very close to the onset of hydrogen adsorption in an acidic medium. Therefore, in this study, the metal surface at 0.3 V/RHE in an acidic medium (pH = 0) is treated as neutral. The influence of pH is captured through its entropic effects on the value of the absolute potential of the reversible hydrogen electrode and, consequently, on the surface charge of the RHE. Thus, at room temperature,

$$\Phi_{\mathrm{RHE}} = \Phi_{\mathrm{SHE}} + \frac{kT}{e} \ln[\mathrm{H}^+] \simeq \Phi_{\mathrm{SHE}} - 0.059 \times p\mathrm{H(V)}.$$

Consequently, the metal surface with the same relative potential of 0.3 V/RHE now bears a nonzero charge density

$$\sigma = -0.059 \times c_{\mathrm{dl}} \times p\mathrm{H}. \quad (4)$$

Using this electrochemical model, $\Delta G(\theta)$ is calculated in acidic (pH = 1) and alkaline (pH = 13) conditions (Fig. 1). Interestingly, changing the pH has almost no effect on adsorption energies on Pt(100), while a sizeable

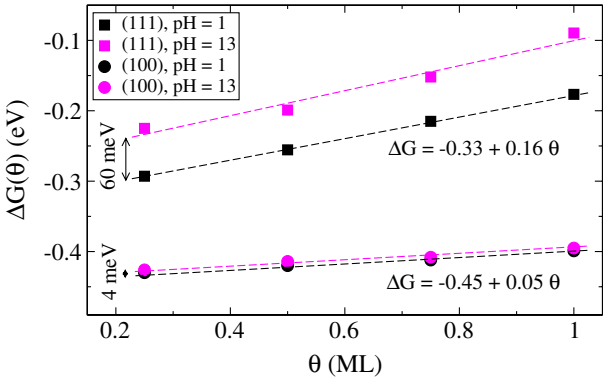

FIG. 1 (color online). Free energy of the $\frac{1}{2}\,\mathrm{H}_2(g) \rightarrow \mathrm{H}^*$ reaction on Pt(111) and Pt(100) for pH = 1 and pH = 13, along with linear fits. The configurational entropy on the surface is not included.

effect is observed on Pt(111). To understand the difference, we plot the electrode absolute potential as a function of hydrogen coverage in Fig. 2. The results for Pt(100) show almost zero slope, suggesting that hydrogen atoms adsorbed on this surface induce only a small change in the surface dipole. By contrast, adsorption of one monolayer (ML) of electropositive hydrogen on Pt(111) lowers the potential by about 0.5 V. We attribute this difference to the more dense packing of the (111) surface, contributing to create more sharply defined planes of "negative" Pt atoms and "positive" H atoms. The link between adsorption energy and surface dipole can be formalized by deriving the adsorbate chemical potential μ_H from the surface free energy. Considering a surface with N hydrogen adsorbates and q free charges, its free energy is

$$G(N, q) = G(N, 0) + \int_0^q \frac{\partial G}{\partial q'} dq' = G(N, 0) + \int_0^q \Phi dq'.$$

Taking the derivative with respect to N to obtain the chemical potential

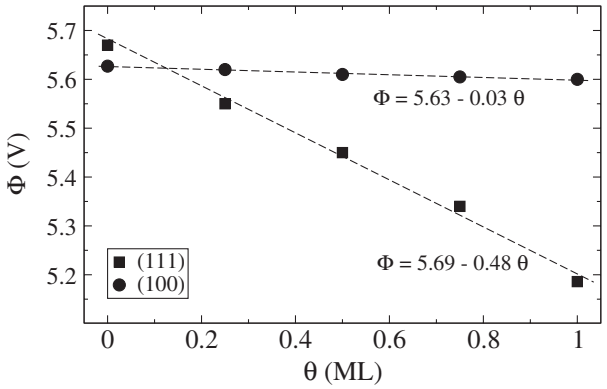

FIG. 2. Electrode absolute potential vs hydrogen surface coverage for Pt(111) and Pt(100), along with linear fits.

$$\mu_H = \frac{\partial G}{\partial N}(N,0) + \int_0^q \frac{\partial \Phi}{\partial N} dq'$$

gives, in terms of the coverage θ and the surface charge density σ

$$\mu_H = \mu_{H,zc} + \frac{1}{\alpha}\int_0^\sigma \frac{\partial \Phi}{\partial \theta} d\sigma',$$

where α denotes the surface atomic density and $\mu_{H,zc}$ is the chemical potential on the neutral surface. If, like in the present case, Φ varies linearly with θ, the previous relation leads to the compact expression

$$\mu_H = \mu_{H,zc} + \frac{\sigma \Delta\chi}{\alpha},$$

where $\Delta\chi$ is the surface dipole change for a full monolayer of hydrogen [-0.03 on (100), -0.48 on (111)]. Using Eq. (4) for σ, the chemical potential change upon variation of pH is finally given by

$$\Delta\mu_H = -0.059 \times \frac{c_{\mathrm{dl}} \Delta p\mathrm{H} \Delta\chi}{\alpha}.$$

This result confirms that the pH dependence of the adsorption energy is directly proportional to the surface dipole induced by adsorbates. Moreover, this effect can be related to the concept of electrosorption valency. The electrosorption valency λ of the proton can be obtained as the number of electrons transferred to the electrode from the external circuit upon adsorption of one proton at constant potential [33]. This is equal to 1 plus a corrective quantity to compensate for the induced change in the surface potential. Adsorption of one proton on a unit surface area perturbs the potential by $\delta\Phi = \frac{\Delta\chi}{\alpha}$, which is compensated by adding $\eta = \frac{c_{\mathrm{dl}}\Delta\chi}{\alpha e}$ electrons to the surface. Consequently, for the chosen value of the capacitance, we have that on Pt(111) $\lambda = 1 + \eta = 0.91$ and that on Pt(100) $\lambda = 0.98$.

Within the underpotential deposition region ($U =$ 0–0.5 V/RHE), the hydrogen surface coverage at equilibrium is obtained by setting $\Delta G_{\mathrm{tot}} = 0$ in Eq. (3) (Figs. 3 and 4). On Pt(111), experimental coverages obtained from integration of voltammetric currents are included for comparison. On Pt(100), integration of the voltammetric current in alkaline conditions is difficult, as it overlaps with the current from OH formation. Therefore, the potential of peak current is used to infer the position of the deposition curve and it appears to be very close to the curve in acidic conditions. The potential at the onset of electrosorption is related to the low-coverage adsorption energy and appears to be well predicted by the Perdew-Burkey-Ernzerhof exchange-correlation functional. On the other hand, the slope of the deposition curve is related to H-H lateral interactions on the surface and they are slightly underestimated on the Pt(111) surface. Of interest is to note the shift of the (111) curve toward lower potentials for higher pH, a direct consequence of the surface dipole effect discussed earlier.

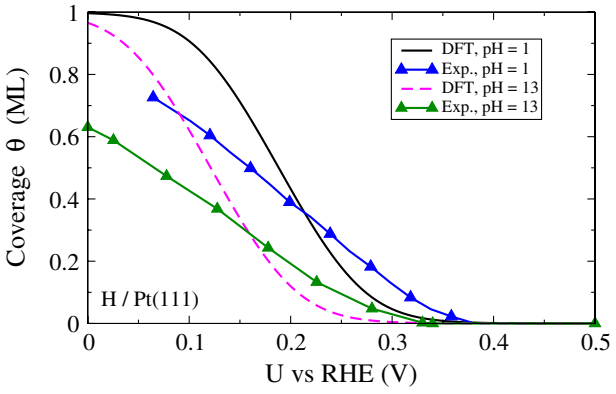

FIG. 3 (color online). Hydrogen deposition on Pt(111) in the low potential region for acidic and alkaline conditions. The experimental data are from Refs. [39,40].

The potential dependence of the surface energy γ in the presence of electrosorbed species can be expressed by the electrocapillary equation [34]

$$d\gamma = \lambda\theta\alpha e dU.$$

In other words, the surface energy can be directly obtained by integrating θ as a function of U from high to low potentials (Fig. 5). The starting point, i.e., the surface energy of the bare facet, is taken from Ref. [35], where the following values are computed with the same formalism used here: $\gamma_{111} = 1.49$ J/m^2 and $\gamma_{100} = 1.81$ J/m^2. We use a simplified model where a Pt nanoparticle only consists of (111) and (100) facets, as suggested by experimental and computational studies [36], and find the energy-minimizing shape by applying the Wulff construction [37]. In this case, a degree of "cubicity" κ can be defined as the ratio of (100) facets over the total nanoparticle surface area that depends only on the surface energy ratio $\frac{\gamma_{111}}{\gamma_{100}}$. As the electrode potential is scanned to

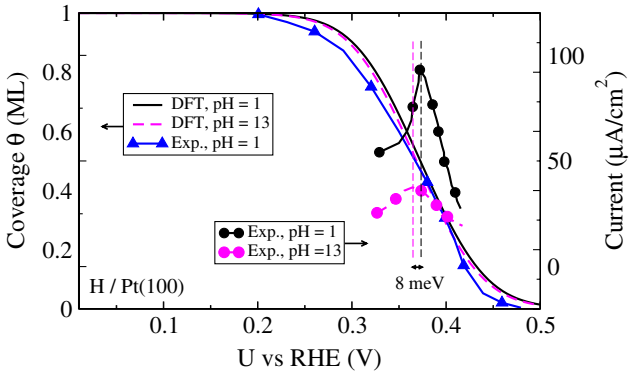

FIG. 4 (color online). Hydrogen deposition on Pt(100) in the low potential region for acidic and alkaline conditions. Integration of the experimental current in the KOH electrolyte (pH = 13) is hindered by overlap with the OH discharge current. The position of the electrosorption curve is then inferred from the potential of peak voltammetric current, which is very close to the value of the same quantity in an acidic medium. The experimental data are from Refs. [39,40].

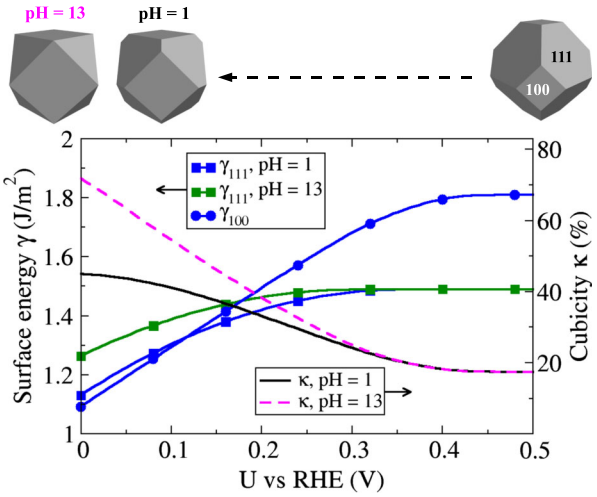

FIG. 5 (color online). Pt(111) and Pt(100) surface energies as obtained from application of the electrocapillary equation to the hydrogen deposition curves for different pHs and changes in the nanoparticle shape, as a function of applied potential.

lower potentials, hydrogen deposition occurs earlier on Pt(100) due to a higher reactivity, leading to a greater stabilization of the surface compared to Pt(111). As a consequence, the equilibrium nanoparticle shape becomes more cubic. In alkaline conditions, that effect is reinforced by the reduced hydrogen binding on Pt(111). The octahedric-to-cubic thermodynamic transition, here quantified for stable Pt nanoparticles, is a phenomenon observed experimentally in slightly different circumstances: It has been shown that hydrogen permeating from the anode to the cathode of a proton exchange membrane fuel cell can reduce Pt ions present in solution and produce nanoparticles having a more pronounced cubic aspect as the hydrogen concentration becomes larger [38].

In summary, we here provide an approach to calculate surface energies and equilibrium shapes of nanoparticles for realistic electrochemical conditions and applied potentials. In the process, we determine surface energies as a function of coverage, chemical potentials as a function of pH, and electrosorption valencies from first principles. We apply this to the study of hydrogen electrodeposition on Pt surfaces, showing how pH indirectly affects adsorbate energies through the surface charge of the RHE interacting with the surface dipole induced by the adsorbates. Derivation of surface energies from electrosorption curves, via the electrocapillary equation, leads to the determination of nanoparticles' equilibrium shapes and shows the ability of the formalism to relate the key factors determining catalytic activity, namely, electric bias, electrolyte pH, adsorbate coverage, surface stability, and catalyst geometry.

We are grateful to Y. Shao-Horn for valuable discussions. This work was supported primarily by the MRSEC Program of the National Science Foundation under Grant No. DMR-0819762.

[1] M. Pourbaix, Corros. Sci. **14**, 25 (1974).
[2] H. A. Gasteiger, S. S. Kocha, B. Sompalli, and F. T. Wagner, Appl. Catal., B **56**, 9 (2005).
[3] H. A. Gasteiger and N. M. Marković, Science **324**, 48 (2009).
[4] J. K. Nørskov, M. Scheffler, and H. Toulhoat, MRS Bull. **31**, 669 (2006).
[5] B. Hammer and J. K. Nørskov, Nature (London) **376**, 238 (1995).
[6] J. Rogal, K. Reuter, and M. Scheffler, Phys. Rev. B **69**, 075421 (2004).
[7] F. Mittendorfer, N. Seriani, O. Dubay, and G. Kresse, Phys. Rev. B **76**, 233413 (2007).
[8] K. Reuter, D. Frenkel, and M. Scheffler, Phys. Rev. Lett. **93**, 116105 (2004).
[9] J. K. Nørskov, J. Rossmeisl, A. Logadottir, L. Lindqvist, J. R. Kitchin, T. Bligaard, and H. Jónsson, J. Phys. Chem. B **108**, 17 886 (2004).
[10] N. M. Marković and P. N. Ross, Surf. Sci. Rep. **45**, 117 (2002).
[11] B. Hammer and J. K. Nørskov, Adv. Catal. **45**, 71 (2000).
[12] J. K. Nørskov, F. Abild-Pedersen, F. Studt, and T. Bligaard, Proc. Natl. Acad. Sci. U.S.A. **108**, 937 (2011).
[13] V. R. Stamenkovic, B. Fowler, B. S. Mun, G. Wang, P. N. Ross, C. A. Lucas, and N. M. Marković, Science **315**, 493 (2007).
[14] C. D. Taylor, S. A. Wasileski, J.-S. Filhol, and M. Neurock, Phys. Rev. B **73**, 165402 (2006).
[15] A. Y. Lozovoi and A. Alavi, Phys. Rev. B **68**, 245416 (2003).
[16] J. Rossmeisl, E. Skúlason, M. E. Björketun, V. Tripkovic, and J. K. Nørskov, Chem. Phys. Lett. **466**, 68 (2008).
[17] M. Otani and O. Sugino, Phys. Rev. B **73**, 115407 (2006).
[18] C. Stoffelsma, P. Rodriguez, G. Garcia, N. Garcia-Araez, D. Strmcnik, N. M. Marković, and M. T. M. Koper, J. Am. Chem. Soc. **132**, 16 127 (2010).
[19] J. Cheng and M. Sprik, Phys. Rev. B **82**, 081406 (2010).
[20] I. Dabo, E. Cancès, Y. Li, and N. Marzari, arXiv:0901.0096v2.
[21] I. Dabo, N. Bonnet, Y. L. Li, and N. Marzari, *Fuel Cell Science: Theory, Fundamentals, and Biocatalysis*, edited by A. Wieckowski and J. Nørskov (Wiley, New York, 2010), Chap. 13.
[22] G. S. Karlberg, T. F. Jaramillo, E. Skúlason, J. Rossmeisl, T. Bligaard, and J. K. Nørskov, Phys. Rev. Lett. **99**, 126101 (2007).
[23] *CRC Handbook of Chemistry and Physics* (CRC Press, Boca Raton, FL, 2004), 84th ed., pp. 5–76.
[24] P. Giannozzi *et al.*, J. Phys. Condens. Matter **21**, 395502 (2009); http://www.quantum-espresso.org.
[25] J. P. Perdew, K. Burke, and M. Ernzerhof, Phys. Rev. Lett. **77**, 3865 (1996).
[26] D. Vanderbilt, Phys. Rev. B **41**, 7892 (1990).
[27] N. Marzari, D. Vanderbilt, A. De Vita, and M. C. Payne, Phys. Rev. Lett. **82**, 3296 (1999).
[28] I. Dabo, B. Kozinsky, N. E. Singh-Miller, and N. Marzari, Phys. Rev. B **77**, 115139 (2008).
[29] D. A. Scherlis, J.-L. Fattebert, F. Gygi, M. Cococcioni, and N. Marzari, J. Chem. Phys. **124**, 074103 (2006).
[30] T. Pajkossy and D. M. Kolb, Electrochim. Acta **46**, 3063 (2001).

[31] M. Otani, I. Hamada, O. Sugino, Y. Morikawa, Y. Okamoto, and T. Ikeshoji, J. Phys. Soc. Jpn. **77**, 024802 (2008).
[32] A. Cuesta, Surf. Sci. **572**, 11 (2004).
[33] R. Jinnouchi, T. Hatanaka, Y. Morimoto, and M. Osawa, Phys. Chem. Chem. Phys. **14**, 3208 (2012).
[34] P. Delahay, *Double Layer and Electrode Kinetics* (Wiley, New York, 1965), Chap. 2.
[35] N. E. Singh-Miller and N. Marzari, Phys. Rev. B **80**, 235407 (2009).
[36] A. S. Barnard and L. Y. Chang, ACS Catal. **1**, 76 (2011).
[37] G. Wulff, Z. Kristallogr. Mineral. **34**, 449 (1901).
[38] J. Ferreira and Y. Shao-Horn, Electrochem. Solid State Lett. **10**, B60 (2007).
[39] N. M. Marković, B. N. Grgur, and P. N. Ross, J. Phys. Chem. B **101**, 5405 (1997).
[40] N. M. Marković, H. A. Gasteiger, and P. N. Ross, J. Phys. Chem. **100**, 6715 (1996).